Full Trajectory Diagnosis of Laser-Driven Radiative Blast Waves in Search of Thermal Plasma Instabilities

A. S. Moore,[1,*] J. Lazarus,[2] T. J. A. Plant,[3] M. Hohenberger,[2] J. S. Robinson,[2] D. R. Symes,[2] M. Dunne,[4] E. T. Gumbrell,[1] and R. A. Smith[2]

[1]*Plasma Physics Division, AWE Aldermaston, RG7 4PR. United Kingdom.*
[2]*Laser Consortium, Blackett Laboratory, Imperial College, London SW7 2BZ. United Kingdom.*
[3]*Ministry of Defence, Foxhill, Bath BA1 5AB. United Kingdom.*
[4]*Central Laser Facility, Rutherford Appleton Laboratory, Oxfordshire OX11 0QX. United Kingdom.*

(Dated: August 7, 2007)

Experimental investigations into the dynamics of cylindrical, laser-driven, high-Mach number shocks are used to study the thermal cooling instability predicted in astrophysical radiative blast waves. A streaked Schlieren technique measures the full blast wave trajectory on a single-shot basis, which is key for observing shock-velocity oscillations. Electron density profiles and deceleration parameters associated with radiative blast waves were recorded, enabling the calculation of important blast wave parameters as a function of time for comparison with radiation hydrodynamics simulations.

PACS numbers: 52.35.Tc, 52.50.Jm, 52.72.+v

An understanding of the role of thermal and dynamical instabilities in plasmas is crucial in creating accurate numerical models of heating and mixing in complex astrophysical systems. In many such systems radiative effects strongly influence the dynamics and can lead to instabilities which are responsible for many of the complex astrophysical structures observed. Radiative blast waves present a physical system that can be instructively studied through observations, numerical modeling and laboratory experiments. Blast waves result when the rarefaction behind a shock front overtakes it, forming a thin shell that contains all the swept-up mass. If the temperature of the post-shock material creates conditions for efficient cooling then energy is radiated through the optically thin shock front. The upstream material is partially preheated, being opaque at some photon energies, but also transmits a considerable fraction of the radiated energy causing the deceleration of the blast wave shell to increase since the system loses energy. In astrophysics this describes the third phase in the evolution of the Supernova Remnant (SNR), the *pressure-driven snowplow*, and it is this radiative phase that has been particularly linked to observed unstable phenomena such as unsteady ultraviolet and optical line emission from the Cygnus Loop and Vela. In the laboratory, hydrodynamic conditions, which may be closely scalable to astrophysics, can be reproduced through utilization of the efficient absorption of high-power, short-pulse laser pulses by atomic clusters [1–3]. This decouples the short-timescale (<ps) cluster expansion from the late-time (many ns) hydrodynamic expansion of interest. Experiments of this type can be used as a powerful aid to understanding astrophysical systems since they enable repeatable access to all phases of the radiation-driven hydrodynamics and have been highlighted as an important area of laboratory astrophysics research [4, 5].

Non-radiative, energy conserving blast waves follow a self-similar expansion as identified by Sedov and Taylor [6]. The blast wave radius R follows a power law in time $R \propto t^n$ in which $n = 0.5$ in cylindrical and 0.4 in spherical geometry. In addition to decelerating more quickly, radiative blast waves can also be identified through observation of an ionized precursor region ahead of the shock front.

Two similar instabilities exist for blast waves in which shock compression is enhanced by the effects of radiation: the dynamical overstability (DO) and the oscillating thermal cooling instability (TCI) [7, 8]. To date experimental research has looked for the effects of the first [2, 9, 10], but the second has not been experimentally investigated and requires a different diagnostic approach. Both mechanisms rely on strong post-shock cooling, but exhibit very different characteristics. The first results from a mismatch in the direction of the thermal and ram pressure vectors either side of the shock and can cause ripples in the position of the shock front to grow. In contrast the TCI depends on the temperature scaling of the cooling function. The cooling function describes the power radiated by a gas of certain density, as a function of electron temperature, and is typically described in terms of a power-law: $\Lambda(T) \propto \rho^2 T^\alpha$, where ρ is the density, T is the temperature and α is the power-law exponent. Provided that $\alpha \equiv d(ln\lambda)/d(lnT) \leq 1$ then the TCI is predicted to cause an oscillation of the shock velocity D [8]. Its occurence is dependent solely on the shape of the cooling function. If a gas radiates more strongly with increasing temperature, the situation can arise where shock-heated gas radiates with such efficiency that the shock front collapses, but is then reformed by the high pressure of the freshly shocked gas. In order to meet these criteria in an astrophysical shock, it has been shown that $D \geq 120\text{km s}^{-1}$, but since the instability is

dependent only on the shape of the cooling function with temperature, and not the absolute temperature, a laboratory experiment to study the same phenomenon can be performed at a significantly lower temperature and thus shock velocity, and still satisfy the inequality for α.

In past experiments blast wave measurements sensitive to the electron density have been performed: interferometry, shadowgraphy or Schlieren imaging [2, 10, 11]. Such experiments enable an estimation of the trajectory through a series of discrete measurements built up over many successive experimental shots. While this is suitable for studying the DO, where single-frame images have shown the break up of the shock front [9], such techniques are inappropriate for investigating the TCI-induced shock front oscillations since very slight shot-to-shot differences in the system dynamics would render such effects invisible to the multi-shot approach. In the past, streaked measurements have been used to study spectral emission from the the blast wave front. Our methodology makes use of this single-shot approach to study shock oscillations and therefore determine key parameters associated with laboratory blast waves in a truly time-dependent fashion.

In this letter we measure the full trajectory of radiative blast waves obtained in argon, krypton and xenon over a 60 ns timescale on a single-shot. We show how this measurement enables us to determine blast wave parameters such as the radiated fraction of energy with considerable accuracy at all stages of the blast wave evolution. In addition we show that although the experiments are well-matched by numerical calculations, they are not able to fully resolve the blast wave position with sufficient detail to confirm the occurence of the TCI.

The experiment consists of a room temperature gas jet containing argon, krypton or xenon at pressures of 59, 41, and 35 bar to keep the different respective mass densities as similar as possible within the limits of cluster formation. The gas jet spray creates an extended target of atomic clusters that is irradiated with a 0.4 J, 700 fs pulse at 1053 nm. Focused to a $20\mu m$ diameter spot of peak intensity $\approx 10^{17}$ Wcm^{-2}, this generates an initial plasma filament of radius $\approx 75\mu$m. At this intensity about 80% of the laser energy is absorbed [3]. In krypton we measure the initial temperature of the plasma using a 16-bit Andor x-ray CCD camera (DX434-BN) operating in a photon counting mode. The bottom inset to Fig. 1 illustrates the typical continuum spectra we recorded from which the initial electron temperature was measured to be $\approx$ 4keV.

An orthogonal, 527 nm, sub-ps probe beam backlights the plasma filament, which is then image-relayed through a Michelson interferometer. By overlaping the image with part of the beam that has not been refracted by the plasma, a single, time-framed image of the spatial profile of electron density is generated [12]. In addition a frequency doubled Nd:YAG (532 nm) was time-

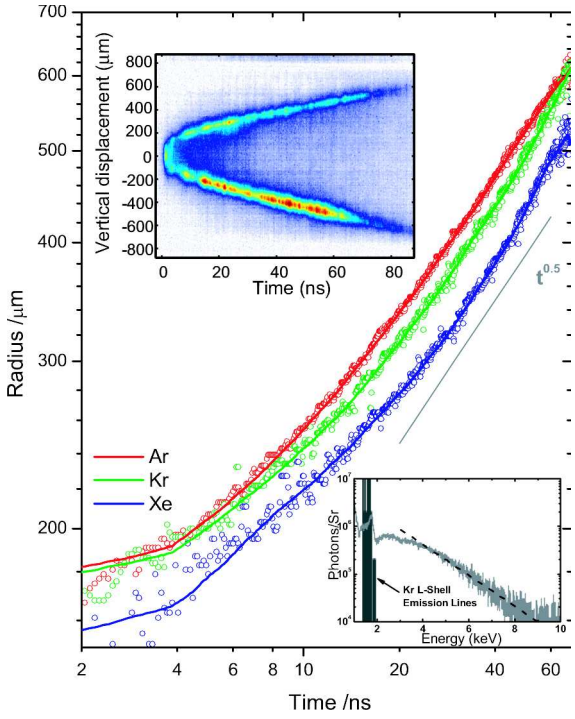


FIG. 1: Measured Blast Wave radius as a function of time in Ar, Kr and Xe. Inset (top) - streaked Schlieren image showing the blast wave obtained on a single laser shot in krypton at 41 bar. Inset (bottom) - X-ray emission spectrum from Kr, indicating an initial electron temperature of $\approx$ 4 keV measured from the continuum slope.

synchronized to the energetic laser pulse to provide a second, long-duration, optical backlighter for streaked Schlieren measurements. This pulse, initially 5 ns in duration, is passed through a low-loss, multiple-reflection etalon generating a pulse of up to 150 ns to illuminate the plasma. A 1 mm stop is placed in the focus of a second low-magnification imaging system to remove the unrefracted probe light, creating a dark-field Schlieren image that is relayed onto a Hadland 675 optical streak camera with $\approx$ 10ps resolution.

This technique allows the blast-wave formation and subsequent trajectory to be tracked on a single shot. By selecting shots within a narrow energy range ($< 10\%$), the electron-density profile of the blast wave can be extracted on consecutive shots using the short-pulse probe. Schlieren imaging, being sensitive to electron density gradients, produces a well-defined image of the steep shock front evolution. This measured evolution is shown in Fig. 1 confirming that between 10 and 25ns, $n < 0.5$. The inset-top shows an example raw streaked image of a blast wave in argon.

The blast wave velocity in xenon, calculated from the trajectory using a 750ps interval, is shown in Fig. 2. For a radiative blast wave profile the regions containing different *effective* polytropic indices are the upstream, post-shock and cavity regions. The properties in each region

can be related given sufficient knowledge of the power-law expansion of the blast wave and the polytropic index in the cavity [13]. From the streaked Schlieren data we obtain the power-law index of the blast wave expansion as a function of time, $n(t) \equiv d(lnR)/d(lnt)$. Without the calculation of the ratio of specific heats in the cavity region performed in Ref. 13, it is conservative to assume $\gamma = 5/3$, which produces an upper limit description of γ in the hot, sparse gas in the interior, and a lower limit of $\varepsilon(t)$ - the radiated fraction of the blast wave kinetic energy.

The Rankine-Hugoniot relations in astrophysics can be generalized for a fully-ionized gas, but in the laboratory ionization will act as an energy sink, since the mean ionization state $\langle Z \rangle$, will change across the shock. This is manifested in our calculation of $\varepsilon(t)$, but is not included in Ref. 13 in which only radiative losses are considered through $0 < \varepsilon < 1$. The lower limit calculated from our data at times exceeds 1, which is likely due to another loss mechanism, such as ionization, and at late times (t >35ns) ε falls below 0 implying that the blast wave gains energy from the previously preheated upstream region in agreement with Ref. 2. In studying an instability which is so closely linked to the form of the cooling function it is important to note that without the separation of ionization and radiative loss mechanisms, through knowledge of $\langle Z \rangle$ either side of the shock front, analytical theories are unlikely to produce close agreement with experiments [14].

To estimate the post-shock temperature we use the radiation-hydrodynamics code NYM [15] to model the experiment, which is run assuming local thermodynamic equilibrium (LTE) with opacities calculated using CASSANDRA [16]. In conjunction with Fig. 1, Fig. 2 indicates that in xenon a blast wave forms at 10 ns, when the radius is ≈ 3 times the deposition region, and is immediately fully radiative ($\varepsilon = 1$) until ≈ 25 ns, at which point the blast wave has cooled sufficiently to stop radiating, and ε drops to zero.

Using NYM in 1D, cylindrical geometry, 420 mJ is deposited into filament of radius of 75 μm, length 3mm and an absorption fraction of between 50 and 80% was assumed to best match the data. The spatial distribution of gas under the jet is approximately Gaussian. The peak density, estimated from the mass flow rate, is $\approx 7 \times 10^{-4}$ gcm^{-3}, but the broad distribution leads to an uncertainty in the uniform density we simulate. Fig. 3(a) shows the measured (gray) and calculated (red) trajectory for Kr, 3(b) shows the measured electron density profile at 25 ns as well as results from different simulations. The best fit to the data (red) was found with laser absorption of 50% and density of 1×10^{-4} gcm^{-3}. From 10 ns, once the blast wave has formed, the simulated trajectory is in very good agreement with that measured, fitting a power-law of $n = 0.456 \pm 0.001$ until 25 ns. No attempt was made to correctly model the data for

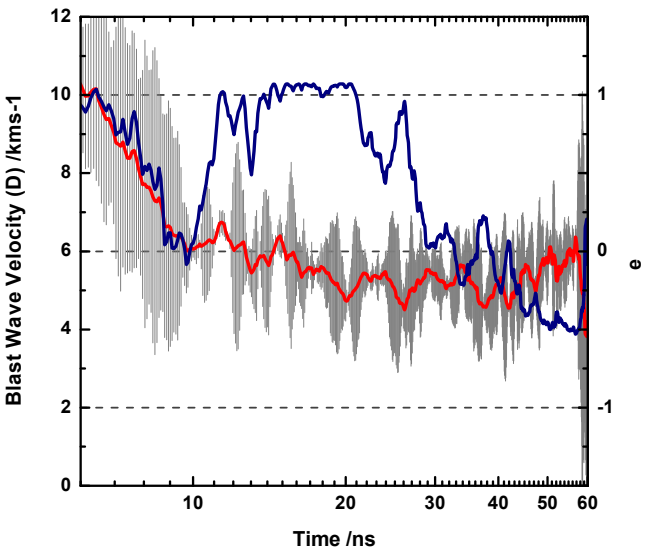


FIG. 2: Blast wave velocity (D) in Xe at 35 bar (red line), error bars in gray. Right axis is the lower-limit value of ε (blue line), indicating the blast wave is fully radiative between 10 and 25 ns.

$t <$ 10ns. Simulated electron density profiles in Fig. 3 demonstrate that artificially turning off radiation causes the shock to propagate further since less energy is lost; in addition, without radiation no precursor forms. Strong radiation is expected to cause further shell-thinning, but interestingly none of the simulations correctly model the thicker shell (FWHM ≈ 50 μm) we observe, all producing a much thinner shell (FWHM $= 20 \pm 3\mu$m). With electron conduction is artifically turned off, the diffusion of free electrons is prevented leaving only convective, fluid forces to act therefore restricting the propagation of the shock front. Overall, while the broad hydrodynamics are successfully reproduced, the detailed cooling in the post-shock cavity region and precursor, which are strongly affected by the ionization and atomic physics, are not adequately treated by assuming LTE.

Occurance of the TCI is critically dependent on the shape of the cooling function as characterised by α. Using the radiative cooling rates calculated in Refs. 17–19 we estimate α. The accuracy with which α can be calculated is limited by the sensitivity of the power-law fit of the cooling function to temperature. We use the polynomial coefficients of cooling functions for each gas, but these are typically only accurate to within a factor of 2. In Xe, published data is only available at $\approx$ 10eV so it is not possible to extrapolate with sufficient accuracy the functionality of the cooling rate coefficient at 3eV.

The values of α in table I indicate that the shock oscillations should be observable in Kr and possibly Xe, but

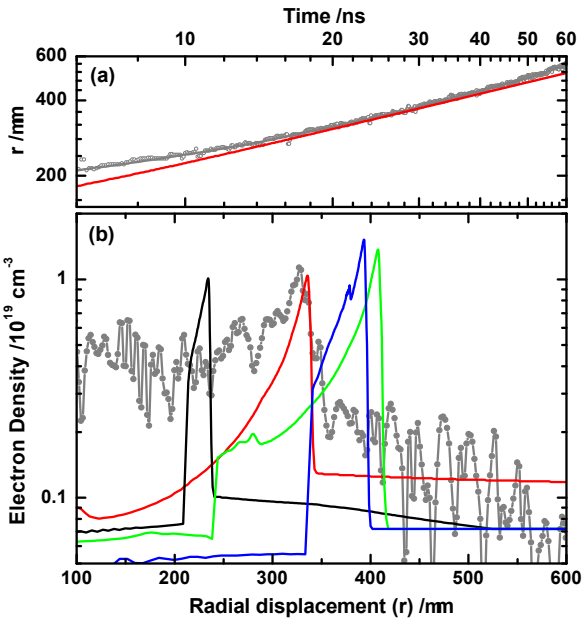


FIG. 3: Blast wave trajectory and electron density measurements and simulations. (a) Streaked Schlieren trajectory measurement in Kr clusters at 41 bar (gray) and simulated trajectory (red). (b) Measured electron density in Kr at 25 ns (gray) and best fit simulation with full electron and radiation transport included (red), electron conduction turned off (black), radiation turned off (green), and both electron and radiation transport turned off (blue).

TABLE I: Estimated range of the power-law exponent α required to fit the cooling function for the approximate temperature range we expect in the post-shock region. Unstable oscillations in the shock front velocity are predicted for $\alpha < 1$ Refs. 20, 21.

Gas	kT_e /eV [a]	D /kms^{-1} [b]	$Mach$	α [c]
Ar	2 ± 0.5	8.2 ± 0.3	40 ± 1	$2.5 \rightarrow 5.1$
Kr	2.5 ± 0.5	7.3 ± 0.7	5 ± 1	$0.6 \rightarrow 1.0$
Xe	3.0 ± 0.5	6.2 ± 0.2	4 ± 2	$-5.0 \rightarrow 3.0$

[a] Postshock electron temperature at 15ns calculated in NYM
[b] Velocity measured at 15 $\pm$0.25ns
[c] Calculated from the coefficients of the polynomial fit to cooling functions in Refs. 18, 19. Values in Xe correspond to kT_e =10eV

not in Ar since $\alpha > 1$. Since the TCI occurs when the shock stalls having radiated the majority of its energy, but then reforms when the dense material in the shell ploughs forward and picks up pre-heated material forming a new shock, an order of magnitude estimate of the oscillation frequency can be made by calculating the time required for all the kinetic energy of the blast wave to be lost through radiation. In Ref. 17 the radiative-cooling loss in xenon at kT_e =7.5 eV and $n_e = 8 \times 10^{18}$ cm^{-3} is quoted as 1.9×10^{-19} ergs.cm^3/s, which if compared with the kinetic energy of the xenon blast wave (4.5×10^4 ergs) corresponds to a cooling time of order 3ns. Despite this being observable on the timescales we measure, we are unable to decern any oscillations within the error of the experiment.

In summary, by means of a new technique we have fully diagnosed the trajectory of high Mach-number radiative blast waves in single-shot experiments. In this way we have investigated the onset of the TCI, but find that we cannot deduce within the current experimental error if the blast waves thus far studied drive the instability according to the predictions of Chevalier and Imamura [8]. This sets an experimental lower limit for the amplitude of shock velocity oscillations that we estimate should occur in Kr and Xe, but not in argon at the temperatures we acheive. Numerical simulations in LTE successfully reproduce the broad electron density profiles and radiative evolution of the blast wave front that we observe but are not successful in matching the precursor or cooling regions. It is therefore unsurprising that the simulations show no evidence of the TCI, and it is expected that non-LTE simulations would be required to show evidence of the TCI in this regime.

We are pleased to acknowledge useful discussions with S. Rose, P. Graham and R. Eagleton, and are grateful for the technical assistance of P. Ruthven, A. Gregory and B. Ratnasekara. This work was supported by EPSRC and MoD UK.

* Electronic address: alastair.moore@physics.org

[1] K. Shigemori, T. Ditmire, B. A. Remington, V. Yanovsky, D. Ryutov, K. G. Estabrook, M. J. Edwards, A. J. MacKinnon, A. M. Rubenchik, K. A. Keilty, et al., The Astrophysical Journal **533**, L159 (2000).
[2] M. J. Edwards, A. J. MacKinnon, J. Zweiback, K. Shigemori, D. Ryutov, A. M. Rubenchik, K. A. Keilty, E. Liang, B. A. Remington, and T. Ditmire, Phys. Rev. Lett. **284**, 1488 (2001).
[3] T. Ditmire, R. A. Smith, J. W. G. Tisch, and M. H. R. Hutchinson, Phys. Rev. Lett. **78**, 3121 (1997).
[4] B. A. Remington, R. P. Drake, and D. D. Ryutov, Rev. Mod. Phys. **78**, 755 (2006).
[5] S. Bouquet, C. Stéhlé, M. Koenig, J. P. Chièze, A. Benuzzi-Mounaix, D. Batani, S. Leyganac, X. Fleury, H. Merdji, C. Michaut, et al., Phys. Rev. Lett. **92**, 225001 (2004).
[6] Y. B. Zel'dovich and Y. P. Raizer, *Physics of of Shock Waves and High-Temperature Phenomena* (Dover Publications, 1966).
[7] E. T. Vishniac, The Astrophysical Journal **274**, 152 (1983).
[8] R. A. Chevalier and J. N. Imamura, The Astrophysical Journal **261**, 543 (1982).
[9] J. Grun, J. Stamper, C. Manka, J. Resnick, R. Burris, J. Crawford, and B. H. Ripin, Phys. Rev. Lett. **66**, 2738

(1991).
[10] A. D. Edens, T. Ditmire, J. F. Hansen, M. J. Edwards, R. G. Adams, P. K. Rambo, L. Ruggles, I. C. Smith, and J. L. Porter, Phys. Rev. Lett. **95**, 244503 (2005).
[11] A. S. Moore, D. R. Symes, and R. A. Smith, Physics of Plasmas **12**, 052706 (2005).
[12] T. Ditmire and R. Smith, Optics Lett. **23**, 618 (1998).
[13] K. A. Keilty, E. P. Liang, T. Ditmire, B. A. Remington, K. Shigemori, and A. M. Rubenchik, The Astrophysical Journal **538**, 645 (2000).
[14] R. P. Drake, *High-Energy-Density Physics* (Springer, 2005).
[15] P. D. Roberts, S. J. Rose, P. C. Thompson, and R. J. Wright, J. Phys. D. **13**, 1957 (1980).
[16] B. J. B. Crowley and J. W. Harris, J. Quant. Spect. Rad. Trans. **71**, 257 (2001).
[17] T. J. Baig and H. J. Kunze, Phys. Rev. E **48**, 2103 (1993).
[18] K. B. Fournier, M. Cohen, M. J. May, and W. H. Goldstein, Atomic Data and Nuclear Data Tables **74**, 333 (1998).
[19] K. B. Fournier, M. J. May, D. Pacella, M. Finkenthal, B. C. Gregory, and W. H. Goldstein, Nuclear Fusion **40**, 847 (2000).
[20] R. S. Sutherland, G. V. Bicknell, and M. A. Dopita, The Astrophysical Journal **591**, 238 (2003).
[21] P. A. Kimoto and D. F. Chernoff, The Astrophysical Journal **485**, 274 (1997).